Influence of the horizontal component of Earth's rotation on wind turbine wakes

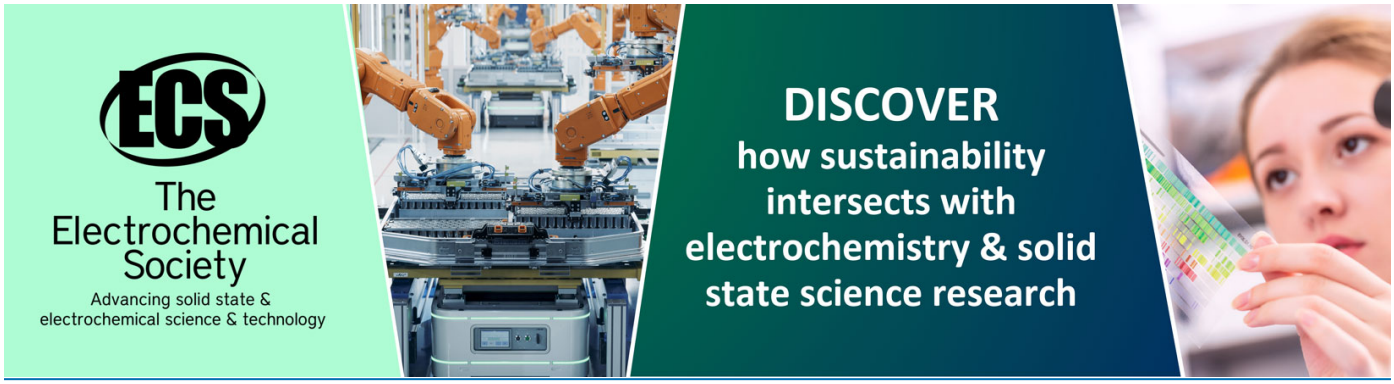

IOP Conf. Series: Journal of Physics: Conf. Series **1037** (2018) 072003 doi:10.1088/1742-6596/1037/7/072003

Influence of the horizontal component of Earth's rotation on wind turbine wakes

Michael F. Howland[1,2], Aditya S. Ghate[1,3], and Sanjiva K. Lele[1,2,3]

1. Center for Turbulence Research, Stanford University, Stanford, CA, USA
2. Department of Mechanical Engineering, Stanford, CA, USA
3. Department of Aeronautics & Astronautics, Stanford, CA, USA

E-mail: mhowland@stanford.edu

Abstract. Wind turbines with large rotor diameters create wakes which are affected by the rotation of the earth. Aside from creating horizontal mean velocity veer, the Coriolis force, caused by earth's rotation, also results in wake deflection and turbulence kinetic energy redistribution. In atmospheric turbulence, the horizontal component of Earth's rotation is often neglected since its forcing magnitude is small compared to buoyant forces. However, at lower latitudes, the horizontal component will cause vertical deflection and redistribution of the same order as the horizontal wake deflection and distribution imposed by the vertical component. Large Eddy Simulations (LES) using uniform laminar inflow, along with more realistic neutrally and stably stratified atmospheric boundary layer inflow conditions are used to study the effect of the horizontal component. Simulations performed at a latitude of 45^0 suggest that the horizontal component cannot be neglected in the study of wind farms since the horizontal component's effect in wind turbine planetary boundary layer flows manifests most directly in the vertical entertainment of kinetic energy. A low-order Coriolis force-induced wake deflection model is proposed and tested against numerical results for uniform inflow conditions.

1. Introduction

With ambitious renewable energy policies nationally and internationally, furthered by the Paris Climate Accord (COP21), the penetration and scale of wind farms are increasing. Due to the experimental difficulty of field experiments of full scale wind farms [1] and the limited Reynolds number realizable in wind tunnels [2], wind farms are often studied using computational fluid dynamics. However, the fully resolved Direct Numerical Simulation (DNS) is computationally intractable at the typical Reynolds numbers within the atmospheric boundary layer [3]. As such, the more computationally feasible approach of large eddy simulation (LES) is generally used [4]. Typically, in a wind farm LES, the simulation is performed in a half channel flow geometry where the mean flow is unidirectional and the Coriolis force is neglected [5, 6]. Neglecting the Coriolis term in the Navier-Stokes equations is typically justified through the nondimensional parameter of the Rossby number: $Ro = G/\omega L$ where G is the geostropic velocity, ω is the rotational rate of the earth, and L is a characteristic length scale (here, L is taken to be D, the turbine diameter). We consider a reference frame such that x corresponds to west-east, y is south-north, and z is perpendicular to the earth's surface. The angular velocity vector for such a frame is $\Omega = \omega \cdot [0\hat{i} + \cos(\phi)\hat{j} + \sin(\phi)\hat{k}]$, where ϕ is the latitude. For wind farms, $Ro \sim O(100 - 1000)$, such that for a fluid parcel, the inertial forces are approximately two or three orders of magnitude larger than the Coriolis.

Recently, the Coriolis term has been introduced and a significant skewing effect has been observed in the wake as a result of the velocity veer [7]. Additionally, the Coriolis force introduces a horizontal wake deflection. The wake deflection based strictly on momentum

deficit at a fixed wall-normal height would be counterclockwise in the northern hemisphere (as seen by an overhead observer), but the influence of vertical momentum transport has resulted an observation of clockwise deflection in a recent Reynolds averaged Navier Stokes study [8]. The influence of the Coriolis force and the statically stabilizing capping inversion upon the vertical transport of kinetic energy has also been studied in wind farms in neutral boundary layers [9]. However, all the studies reported above have neglected the horizontal component of earth's rotation, i.e. $\Omega_2 = 0$ (hereafter referred to as the *f-plane* assumption) without rigorous justification. The horizontal component will result in a positive or negative vertical deflection for a given parcel of fluid depending on the latitude and the flow direction (e.g. westerly or easterly). We further note that while both the transition of a laminar Ekman layer and its turbulence characteristics have been shown to be sensitive to the horizontal component of Earth's rotation (hereafter referred to as the horizontal component) using DNS at lower Reynolds numbers [10, 11], to our knowledge its impact on wind-turbine boundary layers has not been investigated. This is the focus of the present work. The remainder of this paper is organized as follows: in §2.1 the investigation is motivated using a simplified uniform inflow LES test case and in §2.2 a low-order wake deflection model is derived and compared to the LES. Furthermore, in §3, the sensitivity to the horizontal component, is tested in LES of realistic planetary boundary layers. Conclusions are given in §4.

2. Wind turbine array in uniform inflow

In order to characterize the influence of the horizontal component, Ω_2, upon a simplified wind turbine wake, a uniform inflow simulation is performed with an eight turbine wind farm. The influence of Ω_2 in this simplified wake case will provide a motivation to include this term in LES of planetary boundary layers.

2.1. Numerical setup

In order to characterize the effect of the horizontal component Ω_2 on the wake structure and deflection of a wind turbines, we first perform LES of a single turbine and a turbine array in uniform inflow. The Coriolis force presents as a forcing term in the momentum equation of the filtered LES equations. All previous works which have included the Coriolis force in numerical simulations of wind farms have not included the horizontal component Ω_2 which is active in the vertical and west-east momentum equations [7, 8, 9, 12, 13]. The non-dimensional filtered Coriolis forcing terms in the i direction momentum equation with $\Omega_2 = 0$ and $\Omega_2 \neq 0$ are

$$\frac{2\varepsilon_{ij3}\Omega_3}{\omega Ro}\tilde{u}_j^*, \qquad \text{and} \qquad -\frac{2\varepsilon_{ijk}\Omega_j}{\omega Ro}\tilde{u}_k^*, \tag{1}$$

respectively. The nondimensional and filter operators $*$ and $\tilde{\cdot}$ respectively will be excluded for the remainder of the discussion for brevity.

The investigation of the additional forcing implied by equation 1 will be initially motivated through the use of a simplified uniform inflow test case. While uniform inflow lacks the realistic boundary layer features such as shear, turbulent inflow, and veer, it provides a valid but idealized assessment of the momentum balance [14]. The flow is inviscid with the molecular viscosity neglected. Slip walls are used on the top and bottom of the domain and periodic boundary conditions are used in the horizontal direction. A fringe region is used at the exit boundary in the streamwise direction [15]. The uniform inflow has zero free-stream turbulence. An actuator disk model (ADM) turbine is used to represent the turbine forcing with the formulation found in [5]. The domain is rotated such that the flow is perpendicular to the turbine for varying inflow angles. The solver uses Fourier collocation in the horizontal plane, and uses a 6^{th} order staggered compact finite difference scheme in the vertical direction. The sigma subfilter scale model is employed [16] and time stepping is performed using a fourth order Runge-Kutta scheme. The full numerical details of the LES implementation can be found in [17]. For the turbine array cases, the domain is $50D$, $12D$, and $3D$ in the streamwise, spanwise, and wall-normal directions, respectively. The domain is discretized uniformly with 512, 512, and 128 grid points in the three

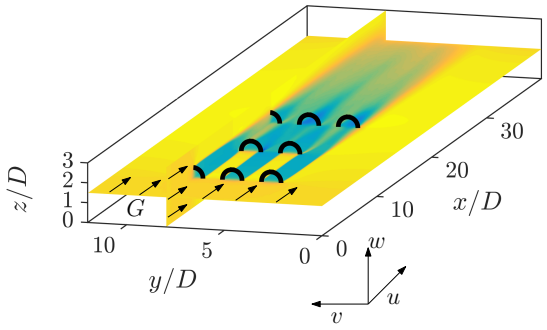

Figure 1. Simulation domain of interest schematic for the uniform inflow cases described in Table 1.

Table 1. Parameters for the uniform inflow turbine array cases. The geostrophic wind direction α is measured from the west-east axis. The Rossby number is fixed at $Ro = 342$ and $\phi = 45°$ for all simulations. The horizontal and vertical wake deflections are y_c and z_c and are computed using the center of mass formulation [18].

Cases	UI	UII	UIII	UIV	UV	UVI
Ω_2	$\cos(\phi)$	0	0	$\cos(\phi)$	$\cos(\phi)$	$\cos(\phi)$
Ω_3	$\sin(\phi)$	0	$\sin(\phi)$	$\sin(\phi)$	$\sin(\phi)$	$\sin(\phi)$
α	0	0	0	90	45	-180
$y_c(x/D = 20)/D$	0.38	0	0.38	0.38	0.38	0.35
$z_c(x/D = 20)/D$	-0.10	0	0	0	0.08	0.10

dimensions. The 8 turbines are placed in three rows, symmetrically in y and z, with the first row located at $x/D = 5$ and spacing of $S_x/D = 7$ and $S_y/D = 2$. The second row has two turbines and is staggered. The flow configuration can be seen in figure 1.

The influence of Ω_2 can be seen in figure 2, where the streamwise velocity downstream of the wind turbine array is shown. The downward vertical deflection manifests as a result of $\Omega_2 \neq 0$. When the f-plane assumption is invoked, case UIII, there is lateral wake deflection but the vertical wake deflection is absent. Notably, when $\Omega_2 \neq 0$, the solution is not invariant to the direction of geostrophic velocity. While there is notable sensitivity to Ω_2 in the present uniform inflow case, this influence must be reviewed in realistic atmospheric conditions (§3).

2.2. Low-order wake deflection model

Previously developed low-order wake models assume the influence of Earth's rotation to be negligible [6, 19]. Here, we model the wake deflection as a result of the Coriolis force as a supplement to the previously developed low-order wake models. Mean wake velocity deficit models are predominantly based on momentum balance. In the uniform inflow cases, the contributions of the Reynolds stresses are not significant in the mean momentum balance since the flow is approximately a laminar wake. Therefore, for the present model, we will neglect the influence of Reynolds stresses which are not readily negligible in realistic boundary layer inflow. Assuming steady state, ADM forcing only in the streamwise direction, neglecting the pressure, Reynolds stress forces, and stratification, the filtered momentum equations become:

$$u_j \frac{\partial u_i}{\partial x_j} = \frac{\varepsilon_{ijk}\Omega_j}{\omega Ro}(G_k - u_k)\,, \tag{2}$$

where all term have been nondimensionalized by G and D. The geostrophic forcing on the right-hand side is the result of the geostrophic pressure balance in the free atmosphere. Taking

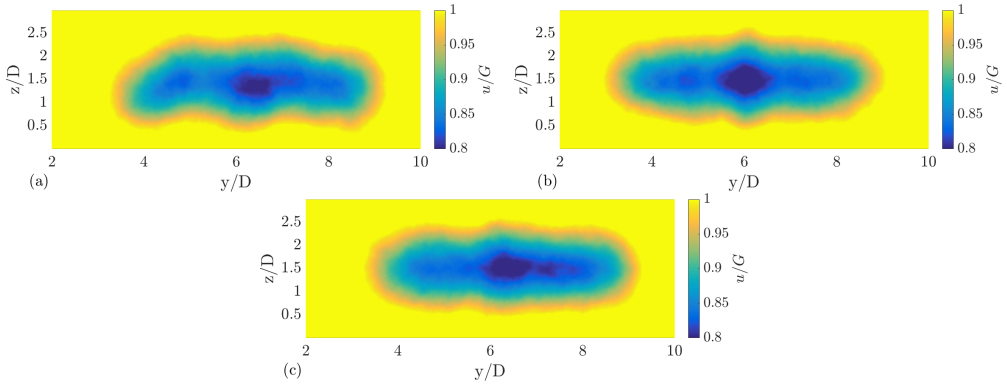

Figure 2. Time averaged streamwise velocity contours $20D$ downstream of the last turbine row. (a) Case UI, $\Omega_{2,3} \neq 0$, (b) Case UII, $\Omega_{2,3} = 0$, and (c) Case UIII, $\Omega_2 = 0$, $\Omega_3 \neq 0$.

G to be strictly west-east ($i = 1$), we can simplify equation 2 for the spanwise and wall-normal directions as

$$\frac{\partial v}{\partial x} = \frac{\sin(\phi)}{uRo}(1-u), \qquad \text{and} \qquad \frac{\partial w}{\partial x} = \frac{-\cos(\phi)}{uRo}(1-u). \tag{3}$$

The velocity deficits are computed using the low-order wake models such as the Jensen model, the Gaussian wake model [19], or the coupled wake boundary layer (CWBL) model [6]. Equation 3 can be integrated spatially to obtain estimates for v and w at each location in the domain. With v and w thus obtained, we may obtain a first order approximation for the wake deflection as a result of the Coriolis forcing. We assume that the local convective velocity is the local velocity such that the time to travel a given fixed distance $\mathrm{d}x$ is $\mathrm{d}t = \mathrm{d}x/u(x,y,z)$ for all locations in the domain. As such, we can estimate the centerline wake deflection as $\Delta y(x,y,z) = v(x,y,z) \cdot \mathrm{d}t + \Delta y(x - \mathrm{d}x, y, z)$ and Δz computed similarly.

For the uniform inflow cases, it is prudent to use the Jensen wake model to characterize the velocity deficits since the turbulence intensity in the wake is small and a "top-hat" profile is appropriate. For the atmospheric boundary layer wake deflection, more sophisticated models such as the Gaussian wake model or the CWBL are appropriate. The wake centers for LES data are computed using a center of mass formulation of [18]. The wake deflections implied by equation 3 and the Jensen wake deficit model are compared to the single turbine and turbine array configurations in figure 3. There is reasonable agreement between LES and the model provided that the wake spreading coefficient k_w is selected appropriately. Here, we select $k_w = 0.05$, which is within the typical range of this parameter [6]. The vertical wake deflection is characterized insufficiently in comparison to the lateral wake deflection. This is likely due to the use of the Jensen model's top-hat velocity deficit profile which is not appropriate even in the present simplified flow.

This model will be of reduced accuracy in planetary boundary layer inflow conditions where the Reynolds stresses cannot be neglected in scaling. Further, this model assumes that the Coriolis effect upon a wind turbine wake is the dominant mechanism of deflection within the flow. Recent work has also noted the influence of the deflection of vertically entrained high momentum flow upon the wind turbine wakes [8].

3. Planetary boundary layers

In order to study the sensitivity of wind turbine wake dynamics to the horizontal component of Earth's rotation, LES studies of realistic planetary boundary layer (PBL) conditions are performed. Three neutral boundary layer simulations and two nocturnal, stable boundary layer cases are performed for a single turbine case. Four neutral boundary layer simulations are performed for a wind turbine array.

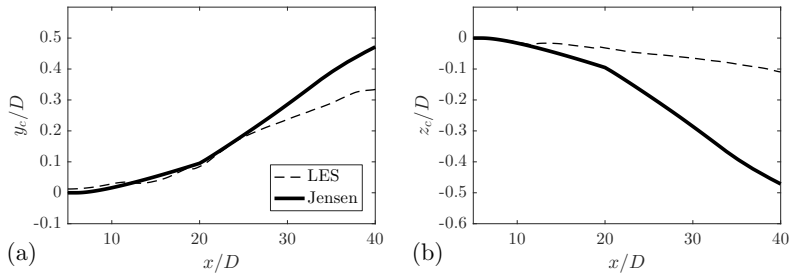

Figure 3. (a) Comparison of the y_c/D wake deflection model given by equation 3 and LES results for the uniform inflow case UI. Wake deflections are normalized by the turbine diameter. The dashed lines are LES and the solid lines are the model. The velocity deficit input to equation 3 is the Jensen model with the wake spreading coefficient $k_w = 0.05$. The first row of turbines is located at $x/D = 5$. (b) Same as (a) for z_c/D.

3.1. Conventionally neutral boundary layer

Recent work has undertaken to study so-called conventionally neutral planetary boundary (CNBL) layers due to the unrealistic nature of truly neutral boundary layers [20]. Such neutral stratification has been the subject of a number of numerical studies of atmospheric boundary layer wind farm interactions [4, 21, 22]. A CNBL is characterized by a boundary layer neutral stratification capped by a stable free atmospheric stratification [23]. Moreover, PBL wind farm interaction studies have shown that the vertical entertainment of kinetic energy is strongly affected by the stable capping inversion which is common in CNBL [9]. Further, gravity waves are excited by the upward displacement of the boundary layer, resulting in power production loss for large wind farms [12, 13]. The horizontal component of Earth's rotation has been neglected in these numerical studies.

In the present study, we aim to measure the influence of the horizontal component in typical CNBL conditions. When $\Omega_2 \neq 0$, the problem is not invariant to the direction of the geostrophic wind. As such, we have performed three CNBL simulations to study the influence of Ω_2. The three single turbine simulations that are carried out represent westerly and easterly flow and are summarized in Table 2. The domain is originally set with the x-axis corresponding to the west-to-east direction and the geostrophic velocity is west-to-east. The latitude is $\phi = 45^\circ$ and the domain extent is $\mathrm{L_x} = 3.2$ km, $\mathrm{L_y} = 1.6$ km, and $\mathrm{L_z} = 1.6$ km. The number of grid points are 512, 256, and 256 in x, y, and z respectively. Periodic boundary conditions are used in the horizontal directions. A sponge is used at the top of the domain to prevent the gravity waves from reflecting back into the computational domain. The Moeng Monin-Obukhov similarity theory based wall model is used with a roughness length of 10 cm [24]. The geostrophic velocity is set to 5 m/s, the lower bound of observed G [25]. The rotor diameter is $D = 126$ m, with a hub height of 100 m, and a coefficient of thrust of $C_T' = 1.33$. This corresponds to a Rossby number based on the rotor diameter of $Ro = 544$. Results are time averaged over four hours of physical time. All result velocities are normalized by the geostrophic velocity.

The wind turbine array simulation shares the domain and precursor simulation as the single turbine cases. The wind turbine array contains a periodic array of 9 turbines aligned with a streamwise spacing of $8.5D$ and a spanwise spacing of $4.2D$.

3.1.1. Precursor simulations The CNBL must reach quasi-statistical stationarity before the wind turbines may be incorporated [15]. Here, we measure quasi-statistical stationarity with u^* and the angle between u and v as a function of time. The velocity field is initialized with uniform inflow in the x direction and zero in y and z with random noise added in all directions. The potential temperature profile is initialized with zero lapse rate from the ground until a height of 700 m and a stable lapse rate of 3 K/km in the free atmosphere. The simulation reaches stationarity in the boundary layer height (measured both in velocity and in temperature as

Table 2. Parameters for the planetary boundary layer cases. Cases with the prefix N and NA are CNBLs with a single turbine and a 9 turbine array respectively. Cases with the prefix G are stable. The surface temperature time rate of change $\partial\theta_s/\partial t$ is given in K/hour and the boundary layer height is initialized as h_{init} in meters. Cases NII, NAII, and GII correspond to the f-plane assumption.

Cases	NI	NII	NIII	NAI	NAII	NAIII	NAIV	GI	GII
$\partial\theta_s/\partial t$	0	0	0	0	0	0	0	-0.25	-0.25
ϕ	45°	45°	45°	45°	45°	45°	45°	45°	45°
Ω_2	$\cos(\phi)$	0	$\cos(\phi)$	$\cos(\phi)$	0	$\cos(\phi)$	$\cos(\phi)$	$\cos(\phi)$	0
Ω_3	$\sin(\phi)$	$\sin(\phi)$	$\sin(\phi)$	$\sin(\phi)$	$\sin(\phi)$	$\sin(\phi)$	$\sin(\phi)$	$\sin(\phi)$	$\sin(\phi)$
α	0	0	$-180°$	0	0	$-180°$	90°	0	0
h_{init}	700	700	700	700	700	700	700	100	100

in [9]) and in the surface friction velocity after approximately four hours of physical time. Numerical experiments show that neglecting Ω_2 for a PBL simulation without wind turbines does not result in statistical differences. Due to the small influence of Ω_2 in a PBL simulation, the same precursor is used for all three CNBL cases. As a result of the Coriolis force, there is a significant wind veer present, measured as $\phi^n = \tan^{-1}(\langle v\rangle / \langle u\rangle)$ where n denotes the time step. The mean profiles of speed, wind veer, and potential temperature are shown in figure 4. Due to the wind veer, which cannot be known a priori, a wind angle controller must be used. Previous works have used proportional-integral (PI) controllers coupled with a Coriolis-like psuedo-force added to the momentum equation [7, 12, 26]. Here, we use integral control of $\vec{\omega}_c$,

$$\vec{\omega}_c = k\left(\phi^n_{z_h} - \phi_{ref,z_h}\right)\hat{k}, \qquad \text{and} \qquad \frac{\mathrm{D}\vec{u}}{\mathrm{D}t} = \mathrm{RHS} - 2\vec{\omega}_c \times \vec{u}, \tag{4}$$

where $\phi^n_{z_h}$ is the wind direction at the wind turbine hub height at time step n, ϕ_{ref,z_h} is the desired wind angle at the hub height, and k is the integrator constant. The control angular velocity is strictly in the $\hat{k}$ vertical direction. The present $k = 2$ minutes^{-1}. Importantly, the geostrophic wind direction and the Coriolis force from earth's rotation must be updated to account added control as $\alpha^{n+1} = \alpha^n - \omega_c \Delta t$. The Euler and centrifugal forces induced by the non-inertial reference frame are added into the pressure term of the momentum equation. Numerical experiments show that the integral controller does not influence the statistics of the flow. The influence of the integral controller on the mean statistics is shown in figure 4.

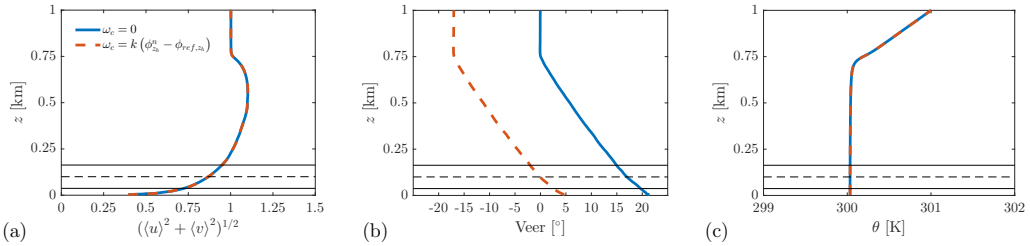

Figure 4. The neutral boundary layer precursor simulation mean (a) speed, (b) wind veer, and (c) potential temperature profiles as a function of the wall-normal distance z. The profiles are averaged over the horizontally homogeneous directions and shown after 7 hours of physical time simulation. The precursor simulation using the integral controller given by equation 4 is also shown.

3.1.2. Single turbine results The expectation from Section 2.1 is that Ω_3 will cause counterclockwise spanwise wake deflection. Additionally, as is clear from equation 2, negative vertical wake deflection is expected for westerly flow and positive vertical wake deflection is expected for easterly flow. No vertical wake deflection is expected for northerly or southerly flow. However, in realistic PBLs, it is not justified to neglect the Reynolds stresses in the derivation of equation 2 and vertical shear and veer introduce more complications. In the present CNBL flows, the wakes do not deflect significantly in either the lateral or vertical direction; $O(0.1D)$ occurs $12D$ downstream of the wind turbine. Since the wake deflection scales with velocity deficit, a compact wind farm will likely have higher wake deflections.

The mean speed deficit profiles can be seen in figure 5, where $\Delta u = (\langle u \rangle^2 + \langle v \rangle^2)^{1/2}_{\infty} - (u^2 + v^2)^{1/2}$ with $(\langle u \rangle^2 + \langle v \rangle^2)^{1/2}_{\infty}$ being the speed at the spanwise extent of the domain. We can make a few observations. First, there is a discrepancy between the three cases in the mean profiles, meaning that the f-plane assumption is not valid in the study of wind turbine wakes in CNBLs. Second, NI has a faster wake recovery than NII or NIII, although the difference is not very strong. This may be due to enhanced vertical entertainment of kinetic energy as a result of $\Omega_2 \neq 0$. Third, NI and NIII bear different wake recovery behavior. Therefore, wind turbine wakes within realistic PBL flows are not inflow direction invariant.

The vertical profiles of the Reynolds shear stress associated with vertical entrainment can be seen in Figure 6. At $5D$ downstream of the turbine, case NI has the largest magnitude of shear stress. The increased magnitude results in an increased vertical transport of kinetic energy. Cases NII and NIII have approximately the same peak magnitude. At $8D$ downstream of the turbine, the peak magnitudes of shear stress are approximately the same in all cases but the peak location for case NI has shifted negatively in the vertical direction. Additionally, there is a distinct secondary peak shear at the bottom of the turbine, characteristic of the shear layer formed by the wind turbine. Case NI has the smallest magnitude of the lower shear peak and case NIII has the largest. The lower peak of shear stress is associated with positive vertical transport and is suppressed in case NI with respect to NII and enhanced in case NIII with respect to NII. Evidently, in the present neutral boundary layer case, negative vertical entrainment is slightly enhanced. The increased intensity of vertical transport likely causes the wake recovery discrepancies seen in figure 5. Such discrepancies between the various cases discussed presently will be more present in a compact wind farm due to the increased turbulent mixing and velocity deficits. However, due to the complexities of wind turbine PBL interactions, the influence of Ω_2 may present differently in a wind farm case versus a single wind turbine case.

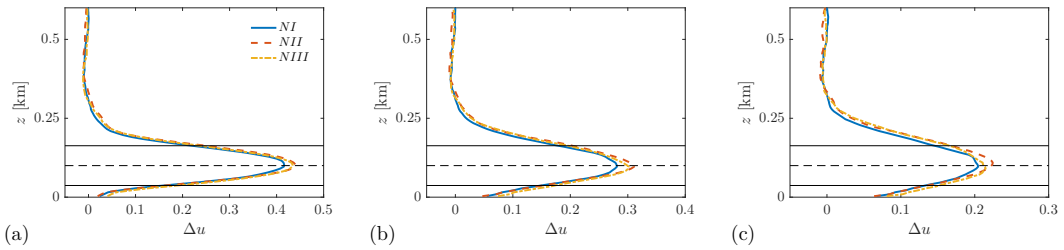

Figure 5. The time averaged single turbine neutral boundary layer vertical profiles of streamwise speed deficit Δu at (a) 3, (b) 5, and (c) 7 diameters downstream.

3.1.3. Wind turbine array results The influence of Ω_2 will be a function, in general, of the effective Rossby number of the flow. Additionally, the influence of Ω_2 is expected to increase with the prevalence of nonzero w, the vertical velocity. For the 9 turbine array, the effective Rossby number has increased compared to the single turbine case due to the larger effective characteristic length scale. Further, more turbines will introduce larger inhomogeneity which will likely influence the vertical momentum balance. The influence of Ω_2 in the CNBL wind turbine array cases can be seen in figure 7. From figure 7(a), we can observe that Ω_2 and α are

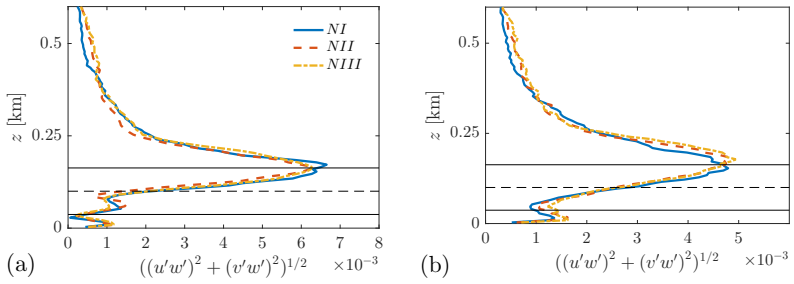

Figure 6. The time averaged single turbine neutral boundary layer vertical profiles of shear stress taken at the spanwise centerline (a) 5 and (b) 8 rotor diameters downstream of the wind turbine.

both relevant to the horizontally averaged mean speed profiles. In particular, Ω_2 significantly affects the geostrophic jet and boundary layer height. The present simulations do not have a strong capping inversion which will likely influence the role of Ω_2 on the mean velocity profiles and boundary layer height [9]. In general, as is clear from equation 1, we expect cases NAI and NAIII to be most different with case NAIV to be an intermediate result. This influence is directly seen in figure 7(b) where the vertical transport is enhanced in case NAIII compared to NAI. The impact upon vertical transport manifests directly on the wake recovery which can be seen in figure 7(c). These results most likely differ from the single turbine case due to the strong influence of Ω_2 on the mean characteristics of the boundary layer which was not present in cases NI-NIII.

The discrepancy between cases NAI and NAIII can be seen directly in the speed deficit contours in figure 8. The horizontal component of Earth's rotation influences the momentum balance in the flow. Since the boundary layer does not grow in case NAI, the wake recovery is slow. In case NAIII, there is prevalent velocity deficit pronounced up to the boundary layer height. This result is expected from equation 1 since a parcel with velocity deficit compared to the geostrophic will result in negative vertical momentum forcing for case NAI and positive vertical momentum forcing for case NAIII. Notably, case NAIV, with $\alpha = 90°$ is not expected to be identically equal to case NAII due to velocity veer.

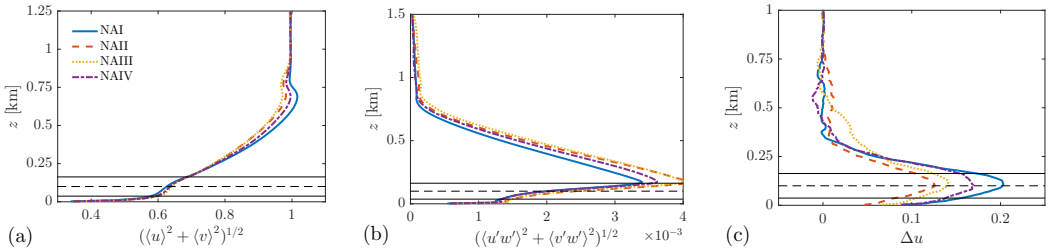

Figure 7. The time and horizontally averaged wind turbine array neutral boundary layer vertical profiles of (a) speed, (b) shear stress, and (c) the time averaged streamwise speed deficit Δu at the centerline $5D$ downstream of the first row of turbines.

3.2. Stable nocturnal boundary layer

The influence of Ω_2 is also tested in stable static stratification. Here, two shallow nocturnal PBLs are simulated with a surface temperature cooling of 0.25 K/hour and an initial boundary layer height of 100 m. The latitude is $\phi = 45°$ and the domain extent is $L_x = 1.6$ km, $L_y = 0.4$ km, and $L_z = 0.4$ km. The grid points are 512, 128, and 128 in x, y, and z respectively. Boundary conditions besides the surface heat flux are shared with the CNBL cases. The two

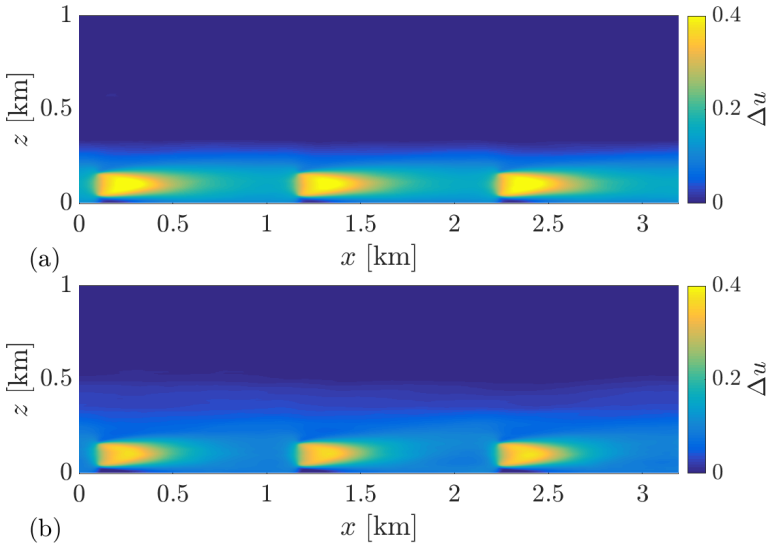

Figure 8. Time averaged streamwise speed deficit Δu at the centerline of the domain for (a) NAI and (b) NAIII.

cases' parameters are summarized in Table 2. The two cases share a precursor simulation which is run for 8 physical hours. The controller given by equation 4 is used to force the inflow angle $\phi^n = 0$ at hub height and time averaging is performed for one hour of physical time. The wind turbine has a hub height of 70 m, a rotor diameter of 80 m, and $C_T' = 1.33$. The turbine is placed 100 m into the streamwise domain and in the center of the spanwise domain. This flow setup is similar to [7] except at $\phi = 45°$. The Rossby number based on the turbine diameter is $Ro = 686$.

3.2.1. Results The comparisons of vertical profiles of shear stress and velocity deficit are shown in figure 9. The differences between GI and GII are less pronounced than NI and NII. This may be due to the decreased Rossby number, increased stabilizing stratification, and increased velocity veer. There are small differences in the shear stress profiles between GI and GII seen in figure 9(a). The peak locations are approximately equal between the two cases and the peak magnitudes are slightly larger in case GII. Wake recovery is slightly faster in case GII (figure 9(b)). In this shallow, stable boundary layer, the velocity veer is significant and wake skewing is pronounced [7].

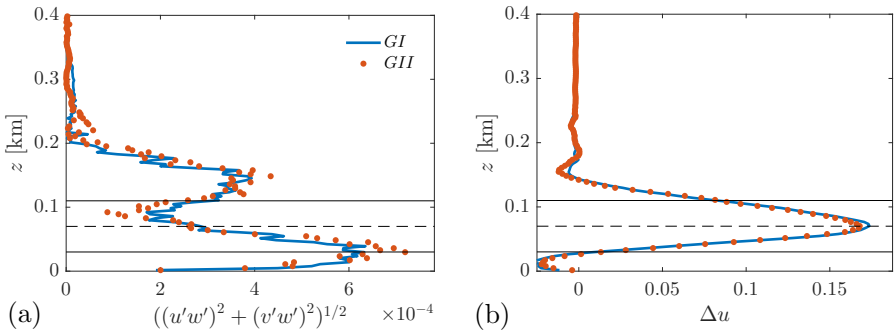

Figure 9. The time averaged stable boundary layer vertical profiles of (a) shear stress taken at the spanwise centerline $8D$ downstream of the wind turbine and (b) centerline velocity deficit $8D$ downstream of the wind turbine.

4. Conclusions

In the present study, we have investigated the influence of the horizontal component of Earth's rotation on wind turbine wakes using uniform and neutral and stable boundary layer inflow conditions. The horizontal component presents in the vertical momentum equation and has often been neglected due to its small magnitude with respect to buoyant forces in PBL flows. However, due to the inhomogeneity introduced by a wind turbine wake, the horizontal component will be relevant to the flow structure of a wind turbine wake at lower latitudes and Rossby numbers. With uniform inflow, which lacks shear or veer, the influence of the horizontal and vertical components of Earth's rotation are of the same order. With neutral boundary layer inflow, the horizontal component impacts the vertical transport of kinetic energy and wake recovery. However, these impacts are less pronounced in the stable, shallow nocturnal boundary layer cases. The influence of Ω_2 is very significant in the CNBL wind turbine array case. Further investigation is required to determine which flow configurations and conditions require $\Omega_2 \neq 0$.

Overall, the horizontal component of Earth's rotation causes wind farms to be inflow direction dependent. Further investigation of the turbulence kinetic energy and Reynolds stress transport budgets are required. In particular, the Coriolis force will act to redistribute Reynolds stresses and the horizontal component may be of notable impact. Future work will focus on the investigation of Reynolds stress transport within wind farms with realistic Coriolis forcing.

Acknowledgements

M.F.H. is funded through a National Science Foundation Graduate Research Fellowship under Grant No. DGE-1656518 and a Stanford Graduate Fellowship. A.S.G is funded via a seed grant provided by Tomkat Center for Sustainable Energy at Stanford University. The simulations were run on Stampede2 supercomputer via a computer time allocation provided by XSEDE (TG-ATM170028).

References

[1] Cal R B, Lebrón J, Castillo L, Kang H S and Meneveau C 2010 *J. of Renew. and Sust. Energy* **2** 013106
[2] Bossuyt J, Howland M F, Meneveau C and Meyers J 2017 *Exp. Fluids* **58** 1
[3] Piomelli U and Balaras E 2002 *Annual Rev. of Fluid Mech.* **34** 349–374
[4] Stevens R J and Meneveau C 2017 *Annual Rev. Fluid Mech.* **49** 311–339
[5] Calaf M, Meneveau C and Meyers J *Phys. Fluids* **22**
[6] Stevens R J, Gayme D F and Meneveau C 2015 *J. of Renew. and Sust. Energy* **7** 023115
[7] Abkar M and Porté-Agel F 2016 *Phys. Fluids* **1** 063701
[8] van der Laan M P and Sørensen N N 2017 *Wind Energy Science* **2** 285
[9] Allaerts D and Meyers J 2015 *Phys. Fluids* **27** 065108
[10] Coleman G N, Ferziger J and Spalart P 1990 *J. Fluid Mech.* **213** 313–348
[11] Leibovich S and Lele S 1985 *J. Fluid Mech.* **150** 41–87
[12] Allaerts D and Meyers J 2017 *J. Fluid Mech.* **814** 95–130
[13] Allaerts D and Meyers J 2018 *Boundary-Layer Met.* **166** 269–299
[14] Martínez-Tossas L A, Churchfield M J and Meneveau C 2015 *Journal of Physics: Conference Series* vol 625 (IOP Publishing) p 012024
[15] Stevens R J, Graham J and Meneveau C 2014 *Renew. Energy* **68** 46–50
[16] Nicoud F, Toda H B, Cabrit O, Bose S and Lee J 2011 *Phys. Fluids* **23** 085106
[17] Ghate A S and Lele S K 2017 *J. Fluid Mech.* **819** 494–539
[18] Howland M F, Bossuyt J, Martínez-Tossas L A, Meyers J and Meneveau C 2016 *J. of Renew. and Sust. Energy* **8** 043301
[19] Bastankhah M and Porté-Agel F 2014 *Renew. Energy* **70** 116–123
[20] Hess G 2004 *Boundary-layer Met.* **110** 319–355
[21] Meyers J and Meneveau C 2012 *Wind Energy* **15** 305–317
[22] Munters W, Meneveau C and Meyers J 2016 *Boundary-layer Met.* **159** 305–328
[23] Esau I 2004 *Annales Geophysicae* vol 22 pp 3353–3362
[24] Moeng C H 1984 *J. of the Atm. Sci.* **41** 2052–2062
[25] Hasse L and Wagner V 1971 *Mon. Wea. Rev* **99** 255–260
[26] Sescu A and Meneveau C 2014 *Quarterly J. of the Royal Met. Society* **140** 2017–2022